




Runaway electron current reconstitution after a nonaxisymmetric magnetohydrodynamic flushChristopher J. McDevitt *Nuclear Engineering Program, University of Florida, Gainesville, Florida 32611, USA*Xian-Zhu Tang *Theoretical Division, Los Alamos National Laboratory, Los Alamos, New Mexico 87545, USA* (Received 3 November 2022; revised 7 June 2023; accepted 21 September 2023; published 16 October 2023)

Benign termination of mega-ampere (MA) level runaway current has been convincingly demonstrated in recent JET and DIII-D experiments, establishing it as a leading candidate for runaway mitigation on ITER. This comes in the form of a runaway flush by parallel streaming loss along stochastic magnetic field lines formed by global magnetohydrodynamic instabilities, which are found to correlate with a low-Z injection that purges the high-Z impurities from a post-thermal-quench plasma. Here, we show the competing physics that govern the postflush reconstitution of the runaway current in an ITER-like reactor where significantly higher current is expected. The trapped “runaways” are found to dominate the seeding for runaway reconstitution, and the incomplete purge of high-Z impurities helps drain the seed but produces a more efficient avalanche, two of which compete to produce a 2–3 MA step in current drop before runaway reconstitution of the plasma current.

DOI: [10.1103/PhysRevE.108.L043201](https://doi.org/10.1103/PhysRevE.108.L043201)

The generation and evolution of runaway electrons (REs) have been extensively studied in a variety of contexts including atmospheric plasmas [1], solar flares [2,3], and magnetic fusion devices [4]. These highly relativistic electrons have recently emerged as a topic of particular interest and importance to the magnetic fusion community. This is due to the possibility that a large population of REs may be inadvertently generated during a tokamak disruption [5]. Due to their high energy, often in excess of 10 MeV, such electrons have the potential to impart substantial damage to plasma facing components (PFCs) [5].

A major step toward mitigating the threat posed by REs has recently been taken. Specifically, recent experiments on JET [6] and DIII-D [7] have shown that (1) a massive injection of deuterium into a post-thermal-quench (post-TQ) plasma can purge the high-Z impurities and subsequently trigger large-scale magnetohydrodynamic (MHD) modes, (2) independent of the specific MHD modes involved, which are different in DIII-D and JET experiments, parallel streaming loss in the resulting stochastic magnetic field leads to the expulsion of a preformed beam of REs, and (3) the spread of the escaping runaways on the PFCs is sufficiently broad such that no appreciable localized heat load is observed. A striking feature of this scheme is its compatibility with a thermal quench in which plasma energy loss is dominated by impurity radiation. The high-Z impurities could be introduced into the plasma accidentally, for example, in the form of a tungsten flake, or deliberately, for example, through pellet injection, to mitigate the thermal loads on the PFC and electromagnetic force loading on the blankets and vacuum vessel [8,9]. The by-product of such strong radiative cooling is a robust Ohmic-to-runaway current conversion. On ITER, a 15 mega-ampere (MA) plasma current discharge could produce a post-thermal-quench

plasma of over 10 MA RE current [5,10–12]. Safely terminating such a large runaway current has been a particularly difficult challenge, for which the three-dimensional (3D) MHD flush of REs associated with the high-Z impurity purge by massive deuterium injection offers an attractive solution.

An issue that is anticipated, but has not materialized with certainty in experiments to date, is the RE current reconstitution after the spontaneous expulsion of REs by the 3D magnetic fields. As long as the flux surfaces heal after the self-excited 3D MHD event, the Ohmic plasma current after the runaway flush is similarly susceptible to Ohmic-to-runaway conversion, just as the plasma is after the initial radiative thermal quench. One difference is the reduced impurity content after the purge due to deuterium injection. If the purge is sufficiently complete and the remnant deuterium density is not too high, Ohmic heating can offset the radiative and transport losses, and reheats the plasma so the parallel electric field $E_{\parallel\eta} = \eta j_{\parallel}$ can drop below the runaway avalanche threshold E_{AV} [13–16]. If this could be maintained over the rest of the current quench, effective runaway “avoidance” would have been achieved. The primary challenge in that scenario becomes a goldilocks requirement on ion densities such that radiative cooling and Ohmic heating would offset each other to lock the plasma to a temperature [17] that is consistent with an Ohmic current decay time in the range of 50–150 ms for ITER [18,19].

In the more conservative and perhaps more likely scenario that the impurity purge is inadequately complete and electron reheating is insufficient to reach $E_{\parallel\eta} < E_{AV}$, the same avalanche physics can drive runaway current reconstitution. The key question becomes how much the plasma current would drop before another Ohmic-to-runaway current conversion is completed. The answer to this question would

dictate the issues one must face in the postflush mitigation designs.

This Letter lays out the fundamental physics considerations underlying the answer to the question of runaway reconstitution after an MHD flush, which are of critical importance to a tokamak reactor such as ITER. The interesting finding is that the runaway current reconstitution follows the same avalanche growth physics as the initial runaway current formation, but the runaway seeding takes place via a new route that makes the runaway reconstitution a far more robust process than the initial runaway plateau formation immediately following the plasma thermal quench. This feature is the “trapped runaway” population in the RE plateau phase that is greatly enhanced by the high- Z impurities before their purge by massive deuterium injection. In a mitigated post-TQ plasma, the electron temperature is radiatively clamped to a very low temperature, possibly in the few eV range. Due to the strong pitch-angle scattering from partially screened weakly ionized impurities (passing) runaways are scattered into the trapped region [20,21]. The radial loss of trapped electrons thus formed, in sharp contrast to that of passing runaways, is insensitive to the stochastic magnetic fields in an MHD event. Furthermore, it is shown below that because of their high energies the trapped runaways are resilient against both collisional slowing down and collisional detrapping [22] during the transition period from the purge to the eventual flux surface rehealing. This plants the seed for a robust runaway reconstitution of the plasma current once the flux surfaces are rehealed after the 3D MHD event.

In a postflush plasma with $E_{||\eta} > E_{AV}$, the runaway current reconstitution follows the same avalanche physics as during the initial formation of the RE plateau, i.e.,

$$I_{RE}^{(\max)} = 2\pi \int_0^a dr r j_{RE}^{(\text{seed})}(r) 10^{|\psi(r)/\psi_{10}(r)|}, \quad (1)$$

which we have written for a simple geometry with circular flux surfaces, r is the radial variable, and a is the minor radius. The amount of poloidal flux required for an order of magnitude increase in runaway population is labeled as $\psi_{10}(r)$. Equation (1) expresses the amount of RE current that could be generated if all of the available poloidal flux were used to amplify the RE seed, and thus corresponds to an upper bound on the amount of RE current that can be generated for a given RE seed $j_{RE}^{(\text{seed})}$. To minimize runaway current reconstitution, one aims for a higher $\psi_{10}(r)$ and a smaller RE seed $j_{RE}^{(\text{seed})}$. A postflush plasma appears to be favorable on both accounts: (1) A reduced high- Z impurity density due to its purge by hydrogen injection increases ψ_{10} [23]; and (2) a lower T_e implies an ineffectiveness of both the Dreicer flux and hot tail formation in seeding the runaways, which points to the most optimistic scenario in which tritium decay and Compton scattering set the minimal runaway seeding in the nuclear phase of ITER. Unfortunately, this optimistic scenario is not fully borne out, where the present Letter demonstrates that magnetic trapping of high-energy electrons provides a robust RE seed.

Magnetic trapping in a stochastic field. Figure 1 shows the average loss time of electrons as a function of their phase space location in a globally stochastic magnetic field. Here, the electron losses are either through spatial transport to the

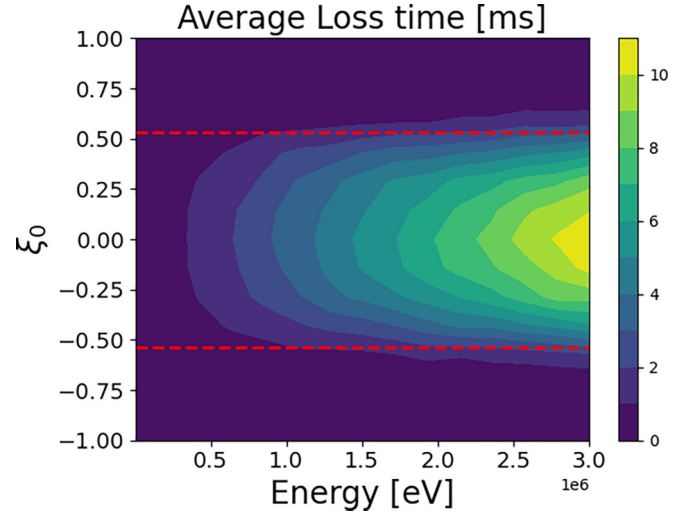


FIG. 1. Average loss time of electrons in an imposed 3D magnetic field. The dashed red lines indicate the location of the trapped-passing boundary. The imposed perturbation has the form $\delta\mathbf{B} = \nabla \times (\alpha \mathbf{B}_{\text{eq}})$, where \mathbf{B}_{eq} is the equilibrium magnetic field, $\alpha = \sum_{m,n} \alpha_{m,n}(r) \cos(m\theta - n\varphi + \delta_{m,n})$, with $n = [1, 6]$, $m = [1, 24]$, and the magnitude of $\alpha_{m,n}(r)$ was increased until a magnetic field without any detectable integrable regions was achieved. The electrons were all initialized at $r/a = 0.5$. The plasma parameters were taken to be $n_D = 5 \times 10^{20} \text{ m}^{-3}$, $E/E_c = 50$, and an ITER-like plasma with $B_0 = 5.3 \text{ T}$ and a minor radius of $a = 200 \text{ cm}$ was assumed.

vessel wall or collisional slowing down to the bulk plasma. It is evident that passing electrons with $|\xi| \gtrsim 0.5$ ($\xi \equiv p_{||}/p$ is the electron’s pitch) are rapidly lost along the open magnetic field lines, but electrons initially located within the trapped region of momentum space remain confined for a far longer period of time [24,25]. This is due to magnetically trapped electrons only following a magnetic field line for a short distance before being reflected and retracing the same magnetic field line, thus sharply limiting their spatial transport. The loss time for such magnetically trapped electrons is largely determined by their detrapping rate. Since the collisional detrapping rate decreases rapidly with the electron’s energy [26], relativistic trapped electrons can remain confined in the plasma for an extended period, even for a fully stochastic magnetic field. This population thus provides a remnant seed capable of surviving global MHD instabilities. A primary aim of this work will be to evaluate the magnitude and decay rate of this seed across a range of plasma conditions, thus providing guidance on what experimental conditions must be achieved to reduce this seed to a specific level.

Self-consistent RE evolution. Our simulation model includes a drift kinetic description of runaway electron evolution [23], which traces the evolution of REs in a toroidal plasma with nested circular flux surfaces, a power balance equation, and a flux diffusion equation. Specifically, for the poloidal magnetic flux ψ ,

$$\left. \frac{\partial \psi}{\partial t} \right|_r = \frac{\eta}{\mu_0} \frac{1}{\langle R^{-2} \rangle} \frac{1}{r} \frac{\partial}{\partial r} \left[r \langle R^{-2} \rangle \frac{\partial \psi}{\partial r} \right] - \frac{\eta}{B_0 R_0} \frac{\langle \mathbf{j}_{RE} \cdot \mathbf{B} \rangle}{\langle R^{-2} \rangle}, \quad (2)$$

with η the background plasma resistivity and $\langle \dots \rangle$ a flux surface average. Ohm’s law takes the form $E_{||} = \eta(j_{||} - j_{RE})$

with j_{RE} the runaway current density. A conducting wall boundary condition $\psi(r=a)=0$ is imposed. This idealized boundary condition prevents external poloidal flux from entering the plasma. The power balance for background plasma follows

$$\frac{3}{2} \frac{\partial p}{\partial t} = \frac{1}{r} \frac{\partial}{\partial r} \left(rn\chi \frac{\partial T_e}{\partial r} \right) - S_{rad}(n_e, T_e) + S_{RE} + \frac{E_{\parallel}^2}{\eta}. \quad (3)$$

Here, electrons, ions, and neutrals are assumed to have the same temperature, $p = n_e T + T \sum_j n_j$ is the total background plasma pressure with the sum over all ion and neutral species, χ is the heat diffusivity taken to be $\chi = 1 \text{ m}^2/\text{s}$, S_{rad} describes radiative losses, S_{RE} is the energy gained by the bulk plasma due to REs slowing down against free electrons [17], and the last term describes Ohmic heating. The charge state and S_{rad} are evaluated using data generated by the collisional radiative code FLYCHK [27] under the assumption of steady state.

Simulation setup. The first step of the simulation study is the preparation of a runaway current plateau. This is obtained through an idealized thermal quench that imposes a cooling history of $T(r, t) = [T_{init}(r) - T_{final}(r)] \exp(-t/\Delta t_{TQ}) + T_{final}(r)$, with the final temperature $T_{final}(r) = T_f [1 - 0.7(r/a)^2]$ and T_f the on-axis temperature after the thermal quench. These initial temperature and density profiles follow $T_{init}(r) = T_0 [1 - 0.7(r/a)^2]^2$ and $n_{e,init}(r) = n_{D,init}(r) = n_{D0} [1 - 0.9(r/a)^2]^{2/3}$, where T_0 and n_{D0} are the on-axis temperature and deuterium density, respectively.

For all cases considered, we will assume $T_0 = 3.1 \text{ keV}$, $T_f = 10 \text{ eV}$, and $n_{D0} = 2.8 \times 10^{13} \text{ cm}^{-3}$. Once the hot tail seed [28–35] has formed, it is amplified by the avalanche mechanism leading to the formation of a RE plateau, where the amount of RE current is controlled by varying the amount of initial plasma current. After the Ohmic to RE current conversion is complete, large quantities of material are injected into the plasma at two different times. During the first injection ($t \approx 18 \text{ ms}$), a variable amount of neon is injected into the RE beam. By injecting the neon into an existing RE beam, we have the freedom to vary the amount of RE current and injected neon independently. Once the neon enters the plasma, the temperature is evaluated via the power balance equation [Eq. (3)]. A second injection composed entirely of deuterium is made later in the simulation ($t \approx 28 \text{ ms}$), resulting in a factor of ten increase in the deuterium density. Shortly after the deuterium injection, a fraction f_{purge} of the initial neon is removed from the plasma in order to describe the purge of high- Z material, a phenomenon observed across a range of experiments [36–39].

Runaway flush and remnant seed. The RE plateau thus formed provides the initial condition for investigating the 3D MHD flush of runaways. Consistent with the toroidally averaged formulation of Eq. (2), we model the enhanced loss of runaways in a globally stochastic magnetic field by a Monte Carlo radial diffusivity of the form

$$D_{RE}^{kin}(\gamma, \xi, r, \theta) = \frac{|v_{\parallel}|}{c} \Theta[|\xi| - \xi_{trap}(r, \theta)] D_{RE}, \quad (4)$$

where $\xi_{trap}(r, \theta) = 1 - B(r, \theta)/B_{max}$, $B(r, \theta)$ is the magnetic field strength at the electron's current location, B_{max} is the maximum value of the magnetic field on the flux surface, and

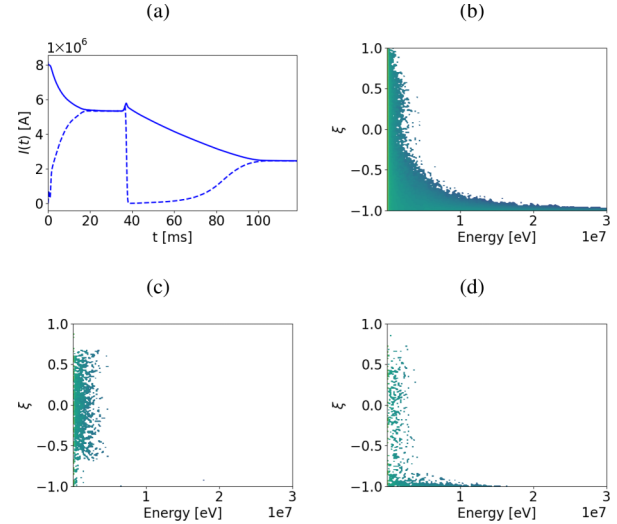


FIG. 2. (a) The evolution of plasma current vs time. The solid curve indicates the total current, whereas the dashed curve indicates the nonthermal current. Time slices of the momentum distribution of REs before [(b) $t - t_{TQ} \approx 33 \text{ ms}$], during [(c) $t - t_{TQ} \approx 39 \text{ ms}$], and after [(d) $t - t_{TQ} \approx 47 \text{ ms}$] the MHD instability. The plasma was assumed to initially carry $I_p \approx 8 \text{ MA}$, a minor radius $a = 200 \text{ cm}$, an on-axis magnetic field $B_0 = 3 \text{ T}$, $f_{purge} = 0.9$, and $\Delta t_{open} \approx 1.43 \text{ ms}$.

$D_{RE} = (1/4)(1/N_t)(a^2/\tau_{transit})$. Here, $\tau_{transit} = 2\pi R_0/c$ is the transit time of a relativistic electron, and $N_{transit}$ is the number of toroidal transits made by a stochastic magnetic field line, where this latter quantity is used to parametrize the strength of the spatial transport. In order to describe the increase in RE transport induced by the large, though transient MHD instability, the diffusivity will be assumed to follow $D_{RE}(t) = D_{RE}^{kin} \exp[-(t - t_{open})^2/\Delta t_{open}^2]$, where t_{open} is the time at which D_{RE} is largest, and Δt_{open} sets the duration of the MHD event.

An example of the impact of a global MHD instability on the phase space distribution of REs is shown in Fig. 2. Here, the MHD instability reaches its peak amplitude at $t \approx 35.8 \text{ ms}$, resulting in the loss of nearly the entire RE current. From Figs. 2(b) and 2(c), it is evident that the expulsion of the relativistic electron population is not complete. In particular, a significant number of trapped relativistic electrons remain confined, providing a seed RE population after the MHD instability ceases. This relativistic population of trapped electrons emerges due to the strong pitch-angle scattering [15,40] coinciding with the presence of a high- Z material such as neon during the current plateau [20,41]. Once the flux surfaces reheat, the detrapping of this remnant population of trapped electrons allows for a sizable RE seed to robustly form [see Fig. 2(d)]. This seed is subsequently amplified by the avalanche mechanism allowing for the partial reformation of the RE plateau. In the following we will identify key parameters that influence $j_{RE}^{(seed)}$ and ψ_{10} , and thus runaway reconstitution.

First, assessing the impact of the duration of the MHD instability Δt_{open} on the size of the remnant seed population, Fig. 3(a) shows the number of energetic electrons that remain confined in the plasma for two different values of Δt_{open} . The shortest value of Δt_{open} is chosen to be comparable to the

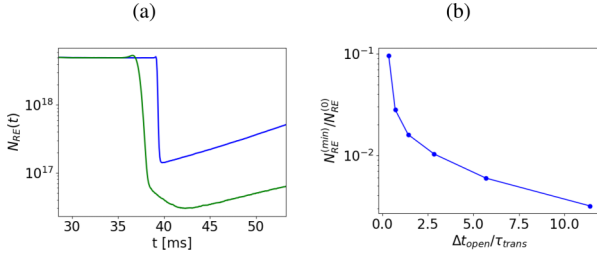


FIG. 3. (a) Shows the evolution of the number of energetic electrons for $\Delta t_{\text{open}} \approx 1.79 \times 10^{-4}$ s (blue curve) and $\Delta t_{\text{open}} \approx 1.43 \times 10^{-3}$ s (green curve). (b) shows the fraction of surviving RE electrons vs the duration of the MHD instability Δt_{open} normalized to the transport timescale $\tau_{\text{trans}} \equiv a^2/D_{\text{RE}}$. The other parameters are $I_p \approx 8$ MA, minor radius $a \approx 200$ cm, $B_0 = 3$ T, $n_{\text{Ne}} = 2n_{\text{D0}}$, and $f_{\text{purge}} = 0.9$.

transport timescale $\tau_{\text{trans}} = a^2/D_{\text{RE}}$ of REs by the 3D magnetic field. For this case, it is evident that the RE population drops sharply during the period of enhanced transport, which is a result of the rapid loss of passing REs. In contrast, considering a case where $\Delta t_{\text{open}} \gg \tau_{\text{trans}}$, the number of REs drops sharply initially, but then decays at a far slower rate, due to the relatively good confinement of trapped relativistic electrons. This transition from a rapid decay rate for $\Delta t_{\text{open}} \lesssim \tau_{\text{trans}}$ to a much slower decay rate for $\Delta t_{\text{open}} \gg \tau_{\text{trans}}$ is evident in Fig. 3(b), where the dependence of $N_{\text{RE}}^{(\text{min})}/N_{\text{RE}}^{(0)}$ on Δt_{open} becomes relatively weak for $\Delta t_{\text{open}} \gg \tau_{\text{trans}}$. From Fig. 3 it is also evident that the RE seed due to remnant trapped electrons ranges between a percent to a tenth of a percent of the original RE beam. Such a seed will thus be orders of magnitude larger than the nuclear seed, which tends to have a magnitude of a few ampere [12].

Runaway reconstitution. Consider now the impact of the amount of neon remaining in the plasma after the deuterium injection. Three cases with different values of f_{purge} are indicated in Fig. 4. Here, it is apparent that in all three cases a similar amount of RE current is able to reform. The origin of this apparent insensitivity is the result of two partially offsetting physical processes. The first is that the amount of impurities that remain in the plasma increases the detrapping rate of the remnant population. This occurs partially due to the higher neon content directly increasing the detrapping rate.

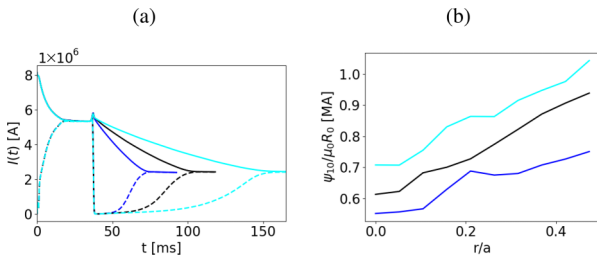


FIG. 4. Evolution of the plasma current [(a)] and the inferred ψ_{10} [(b)] for different purge fractions f_{purge} . The solid curves indicate the total current, whereas the dashed curves indicate the nonthermal current. The blue curves are for $f_{\text{purge}} = 0.6$, the black curves are for $f_{\text{purge}} = 0.9$, and the cyan curves are for $f_{\text{purge}} = 0.975$. The other parameters are, $I_p \approx 8$ MA, minor radius $a \approx 200$ cm, $B_0 = 3$ T, $n_{\text{Ne}} = 2n_{\text{D0}}$, and $\Delta t_{\text{open}} \approx 1.43$ ms.

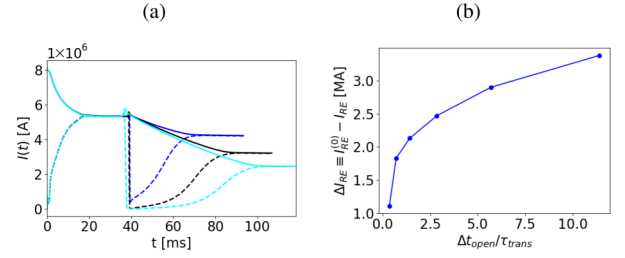


FIG. 5. Current evolution [(a)] and the size of the plasma current drop vs the timescale the flux surfaces remain open [(b)] plotted on a linear scale. The solid curves indicate the total current, whereas the dashed curves indicate the nonthermal current. The curves correspond to $\Delta t_{\text{open}} \approx 0.09$ ms (blue curve), $\Delta t_{\text{open}} \approx 0.36$ ms (black curve), and $\Delta t_{\text{open}} \approx 1.43$ ms (cyan curve). The initial neon density was $n_{\text{Ne0}} = 2n_{\text{D0}} = 5.6 \times 10^{13}$ cm $^{-3}$, $a = 200$ cm, $B_0 = 3$ T, and $\tau_{\text{trans}} \equiv a^2/D_{\text{RE}} \approx 0.26$ ms.

A more subtle mechanism results from the larger inductive electric field present in the higher neon density case, due to the plasma being radiatively pinned to a lower temperature. This larger inductive electric field induces a Ware pinch [42] of the trapped electron population, which convects the electrons inward where they are more easily detrapped. Hence, the retention of neon in the plasma leads to a reduction of the remnant seed population. In contrast, the presence of neon increases the efficiency of the avalanche mechanism. This trend is shown in Fig. 4(b), where as the quantity of neon is increased, the value of ψ_{10} decreases, implying less poloidal flux is required to increase the RE population. For the present example, these competing effects largely offset, yielding a weaker than expected sensitivity to f_{purge} .

Finally, we will investigate the impact of the duration of the MHD event on runaway reconstitution. The amount of reformed RE current for three different values of Δt_{open} is shown in Fig. 5(a). When increasing Δt_{open} from 0.09 to 1.43 ms, the amount of reformed RE current is observed to decrease from 3.9 to 2.0 MA. Hence, while the timescale that the flux surfaces remain open is increased by a factor of 16, the amount of reformed RE current is only reduced by roughly a factor of 2. This relative insensitivity is due to the slow decay rate of the trapped remnant energetic electron population, along with the exponential dependence of the avalanche amplification mechanism on the amount of poloidal flux consumed. The resulting drop in RE current as a function of Δt_{open} is shown in Fig. 5(b), where it is apparent that the current drop becomes a weak function of Δt_{open} once $\Delta t_{\text{open}} \gg \tau_{\text{trans}}$.

Discussion. Runaway reconstitution after a 3D MHD flush is surprisingly robust because of an alternate seeding mechanism via “trapped runaways.” While the size of this seed varies with the amount of neon initially injected into the plasma, the purge fraction, and the time (Δt_{open}) that flux surfaces remain open, its decay is ultimately set by the detrapping from a combination of pitch-angle scattering and the Ware pinch. For the range of parameters considered here, the magnitude of this trapped remnant seed ranged from roughly 1% to 0.1% of the initial RE population. For most cases of interest $\psi_{10}/\mu_0 R_0 \lesssim 1$ MA, so runaway reconstitution comes with a 2–3 MA plasma current drop. Impeding runaway

reconstitution depends on (1) enhancing the detrapping rate and (2) prolonging Δt_{open} . Increasing the postpurge n_D is a straightforward approach for (1), although it is constrained by the assimilation of injected deuterium into the plasma and the density window [7,43] identified for triggering the 3D MHD flush. Experimental studies reveal a significant variation in Δt_{open} [7], but the precise control knob remains to be understood. A more reliable alternative is a passive runaway coil [44–46] that could hold the flux surfaces open for a far longer time period. For detailed scenario modeling for specific tokamak machines, it is important to explicitly follow the 3D MHD mode evolution and the full vertical displacement event (VDE) dynamics, as well as the impurity purge by massive deuterium injection. These are high-priority disruption modeling improvements in next-step research.

Acknowledgments. We thank the U.S. Department of Energy Office of Fusion Energy Sciences and Office of Advanced Scientific Computing Research for support under the Tokamak Disruption Simulation (TDS) Scientific Discovery through Advanced Computing (SciDAC) project, and the Base Theory Program, both at Los Alamos National Laboratory (LANL) under Contract No. 89233218CNA000001. This research used resources of the National Energy Research Scientific Computing Center (NERSC), a U.S. Department of Energy Office of Science User Facility operated under Contract No. DE-AC02-05CH11231 and the Los Alamos National Laboratory Institutional Computing Program, which is supported by the U.S. Department of Energy National Nuclear Security Administration under Contract No. 89233218CNA000001.

-
- [1] J. R. Dwyer and M. A. Uman, *Phys. Rep.* **534**, 147 (2014).
- [2] G. D. Holman, in *Symposium-International Astronomical Union* (Cambridge University Press, Cambridge, UK, 1985), Vol. 107, pp. 191–196.
- [3] M. J. Aschwanden, *Space Sci. Rev.* **101**, 1 (2002).
- [4] H. Knoepfel and D. Spong, *Nucl. Fusion* **19**, 785 (1979).
- [5] T. Hender, J. Wesley, J. Bialek, A. Bondeson, A. Boozer, R. Buttery, A. Garofalo, T. Goodman, R. Granetz, Y. Gribov *et al.*, *Nucl. Fusion* **47**, S128 (2007).
- [6] C. Reux, C. Paz-Soldan, P. Aleynikov, V. Bandaru, O. Ficker, S. Silburn, M. Hoelzl, S. Jachmich, N. Eidietis, M. Lehnen *et al.*, *Phys. Rev. Lett.* **126**, 175001 (2021).
- [7] C. Paz-Soldan, C. Reux, K. Aleynikova, P. Aleynikov, V. Bandaru, M. Beidler, N. Eidietis, Y. Liu, C. Liu, A. Lvovskiy *et al.*, *Nucl. Fusion* **61**, 116058 (2021).
- [8] R. A. Pitts, S. Carpentier, F. Escourbiac, T. Hirai, V. Komarov, S. Lisgo, A. Kukushkin, A. Loarte, M. Merola, A. S. Naik *et al.*, *J. Nucl. Mater.* **438**, S48 (2013).
- [9] M. Sugihara, M. Shimada, H. Fujieda, Y. Gribov, K. Ioki, Y. Kawano, R. Khayrutdinov, V. Lukash, and J. Ohmori, *Nucl. Fusion* **47**, 337 (2007).
- [10] ITER Physics Expert Group on Disruptions, Plasma Control, and MHD and ITER Physics Basis Editors, *Nucl. Fusion* **39**, 2251 (1999).
- [11] J. Martín-Solís, A. Loarte, and M. Lehnen, *Nucl. Fusion* **57**, 066025 (2017).
- [12] O. Vallhagen, O. Embreus, I. Pusztai, L. Hesslow, and T. Fülöp, *J. Plasma Phys.* **86**, 475860401 (2020).
- [13] M. Rosenbluth and S. Putvinski, *Nucl. Fusion* **37**, 1355 (1997).
- [14] P. Aleynikov and B. N. Breizman, *Phys. Rev. Lett.* **114**, 155001 (2015).
- [15] L. Hesslow, O. Embreus, A. Stahl, T. C. DuBois, G. Papp, S. L. Newton, and T. Fülöp, *Phys. Rev. Lett.* **118**, 255001 (2017).
- [16] C. J. McDevitt, Z. Guo, and X.-Z. Tang, *Plasma Phys. Controlled Fusion* **60**, 024004 (2018).
- [17] C. J. McDevitt, X. Tang, C. Fontes, P. Sharma, and H.-K. Chung, *Nucl. Fusion* **62**, 112004 (2022).
- [18] M. Lehnen, K. Aleynikova, P. Aleynikov, D. Campbell, P. Drewelow, N. Eidietis, Y. Gasparyan, R. Granetz, Y. Gribov, N. Hartmann *et al.*, *J. Nucl. Mater.* **463**, 39 (2015).
- [19] E. M. Hollmann, P. B. Aleynikov, T. Fülöp, D. A. Humphreys, V. A. Izzo, M. Lehnen, V. E. Lukash, G. Papp, G. Pautasso, F. Saint-Laurent *et al.*, *Phys. Plasmas* **22**, 021802 (2015).
- [20] C. J. McDevitt, Z. Guo, and X.-Z. Tang, *Plasma Phys. Controlled Fusion* **61**, 024004 (2019).
- [21] Y.-K. Zhang, R.-J. Zhou, L.-Q. Hu, M.-W. Chen, Y. Chao, J.-Y. Zhang, and P. Li, *Chin. Phys. B* **30**, 055206 (2021).
- [22] K. Särkimäki, J. Artola, M. Hoelzl, and the JOEUK Team, *Nucl. Fusion* **62**, 086033 (2022).
- [23] C. J. McDevitt, Z. Guo, and X. Z. Tang, *Plasma Phys. Controlled Fusion* **61**, 054008 (2019).
- [24] H. E. Myrick and J. A. Krommes, *Phys. Rev. Lett.* **43**, 1506 (1979).
- [25] B. D. G. Chandran and S. C. Cowley, *Phys. Rev. Lett.* **80**, 3077 (1998).
- [26] P. Helander and D. J. Sigmar, *Collisional Transport in Magnetized Plasmas* (Cambridge University Press, Cambridge, UK, 2002).
- [27] H.-K. Chung, M. Chen, W. Morgan, Y. Ralchenko, and R. Lee, *High Energy Density Phys.* **1**, 3 (2005).
- [28] S. Chiu, M. Rosenbluth, R. Harvey, and V. Chan, *Nucl. Fusion* **38**, 1711 (1998).
- [29] P. Helander, H. Smith, T. Fülöp, and L.-G. Eriksson, *Phys. Plasmas* **11**, 5704 (2004).
- [30] H. M. Smith and E. Verwichte, *Phys. Plasmas* **15**, 072502 (2008).
- [31] A. Stahl, O. Embreus, G. Papp, M. Landreman, and T. Fülöp, *Nucl. Fusion* **56**, 112009 (2016).
- [32] A. Matsuyama and M. Yagi, *Plasma Fusion Res.* **12**, 1403032 (2017).
- [33] M. Hoppe, O. Embreus, and T. Fülöp, *Comput. Phys. Commun.* **268**, 108098 (2021).
- [34] M. Yang, P. Wang, D. del Castillo-Negrete, Y. Cao, and G. Zhang, *arXiv:2306.05580*.
- [35] C. J. McDevitt, X.-Z. Tang, C. J. Fontes, P. Sharma, and H.-K. Chung, *Nucl. Fusion* **63**, 024001 (2023).
- [36] D. Shiraki, N. Commaux, L. Baylor, C. Cooper, N. Eidietis, E. Hollmann, C. Paz-Soldan, S. Combs, and S. Meitner, *Nucl. Fusion* **58**, 056006 (2018).
- [37] G. Pautasso, M. Dibon, M. Dunne, R. Dux, E. Fable, P. Lang, O. Linder, A. Mlynek, G. Papp, M. Bernert *et al.*, *Nucl. Fusion* **60**, 086011 (2020).

- [38] E. M. Hollmann, I. Bykov, N. Eidietis, J. Herfindal, A. Lvovskiy, R. Moyer, P. Parks, C. Paz-Soldan, A. Y. Pigarov, D. Rudakov *et al.*, *Phys. Plasmas* **27**, 042515 (2020).
- [39] C. Reux, C. Paz-Soldan, N. W. Eidietis, M. Lehnen, P. Aleynikov, S. A. Silburn, V. K. Bandaru, O. Ficker, M. Hoelzl, E. M. Hollmann *et al.*, *Plasma Phys. Controlled Fusion* **64**, 034002 (2022).
- [40] L. Hesslow, O. Embréus, M. Hoppe, T. DuBois, G. Papp, M. Rahm, and T. Fülöp, *J. Plasma Phys.* **84**, 905840605 (2018).
- [41] C. Liu, D. P. Brennan, A. Lvovskiy, C. Paz-Soldan, E. D. Fredrickson, and A. Bhattacharjee, *Nucl. Fusion* **61**, 036011 (2021).
- [42] A. Ware, *Phys. Rev. Lett.* **25**, 15 (1970).
- [43] A. Battey *et al.*, Passive and active remitigation tools under development at DIII-D, 9th Runaway Electron Modelling (REM) meeting (2022), <https://ft.nephy.chalmers.se/?p=confagenda&id=3> (unpublished).
- [44] A. H. Boozer, *Plasma Phys. Controlled Fusion* **53**, 084002 (2011).
- [45] D. B. Weisberg, C. Paz-Soldan, Y. Liu, A. Welander, and C. Dunn, *Nucl. Fusion* **61**, 106033 (2021).
- [46] R. Tinguely, V. Izzo, D. Garnier, A. Sundström, K. Särkimäki, O. Embréus, T. Fülöp, R. Granetz, M. Hoppe, I. Pusztai *et al.*, *Nucl. Fusion* **61**, 124003 (2021).